Journal of Power Sources 236 (2013) 192–199

Contents lists available at SciVerse ScienceDirect

Journal of Power Sources

journal homepage: www.elsevier.com/locate/jpowsour

Effect of porous interlayer on the long-term stability of $(La_{0.8}Sr_{0.2})_{0.97}MnO_3$ cathode for solid oxide fuel cells

Jun Yang, Hiroki Muroyama, Toshiaki Matsui, Koichi Eguchi*

Department of Energy and Hydrocarbon Chemistry, Graduate School of Engineering, Kyoto University, Kyoto 615-8510, Japan

HIGHLIGHTS

- ► Long-term stability of LSM cathode was improved by using a porous interlayer.
- ► The microstructure of the cathode–interlayer interface was quantitatively evaluated.
- ► Active TPB length ratio of the LSM cathode was preserved by using porous interlayer.
- ► LSM cathode with an SDC interlayer showed remarkable long-term stability.
- ► Nanosized Ce-rich particles were observed on the grain boundary LSM cathode.

ARTICLE INFO

Article history:
Received 26 November 2012
Received in revised form
5 February 2013
Accepted 22 February 2013
Available online 4 March 2013

Keywords:
Solid oxide fuel cells
Strontium-doped lanthanum manganite
Strontium-doped ceria
Microstructure
Interlayer
FIB-SEM

ABSTRACT

In this work, the effect of porous interlayer on the microstructural change of LSM cathodes and yttria-stabilized zirconia (YSZ) electrolyte was investigated under a current-accelerated condition at 1000 °C. The polarization resistance of LSM cathode on bare yttria-stabilized zirconia (YSZ) electrolyte decreased significantly after discharge at 1.2 A cm^{-2} for 5 h, and then started to increase gradually. However, when a porous YSZ interlayer was employed between LSM cathode and YSZ electrolyte, the polarization resistance did not increased even after discharge at the same condition for 40 h. The performance changes of the two kinds of cathodes were related with the microstructural change of the interface between LSM cathode and YSZ interlayer. Quantitative analysis for the microstructural change of LSM cathode on YSZ interlayer revealed that even after discharge at 1.2 A cm^{-2} for 40 h, 90% of the triple phase boundary of LSM, YSZ and gas phase remained active for oxygen reduction reaction. On the other hand, the LSM cathode on YSZ electrolyte with a porous Sm-doped ceria interlayer showed remarkable long-term stability even after discharge at 1.2 A cm^{-2} for 160 h.

1. Introduction

Strontium-doped lanthanum manganite (LSM) has high electrical conductivity, excellent activity for oxygen reduction reaction, and close thermal expansion coefficient to yttria-stabilized zirconia (YSZ) electrolytes at high temperatures. Therefore, it is one of the most promising candidates of cathode materials for solid oxide fuel cells (SOFCs) with zirconia electrolytes [1–3]. In spite of high electronic conductivity, the ionic conductivity of LSM is as low as 10^{-7}–10^{-6} S cm^{-1} at 1000 °C [4]. As a result, the electrochemically active sites for oxygen reduction reaction in the LSM/YSZ system are restricted in the triple phase boundary (TPB) of LSM, YSZ, and atmosphere. Hence the length of TPB is closely related to the performance of LSM cathode.

By using focused ion beam-scanning electron microscopy (FIB-SEM), the microstructure of the LSM/YSZ interface can be three-dimensionally reconstructed and the length of TPB can be calculated. Recently, our group conducted a series of quantitative studies on the microstructural change in the LSM/YSZ interface under cathodic polarization with the aid of FIB-SEM technology. It was reported that the apparent TPB length of LSM/YSZ interface increased by 36% after the cathodic current passage of 200 mA cm^{-2} for 300 min at 1000 °C. However, the active TPB length only increased by 7% because most of the increased TPB was among LSM, YSZ, and newly-formed closed pores. The driving force of the formation of the closed pores is still unknown [5]. Furthermore, we conducted similar cathodic polarization on LSM cathode with YSZ electrolyte under current-accelerated condition and a peculiar phenomenon was observed. A dense layer of LSM with a thickness of ca. 1 μm and a great number of closed pores were observed at the LSM/YSZ interface after discharge at 1.2 A cm^{-2} for 40 h.

* Corresponding author.
E-mail address: eguchi@scl.kyoto-u.ac.jp (K. Eguchi).

0378-7753/$ – see front matter © 2013 Elsevier B.V. All rights reserved.
http://dx.doi.org/10.1016/j.jpowsour.2013.02.063

The newly-formed LSM layer covered the surface of YSZ, and decreased the active TPB length from ca. 100% to ca. 29%. As a result, the performance of LSM cathode decreased significantly [6]. These results reveal that the microstructure of LSM/YSZ interface changes significantly due to cathodic polarization, and will cause degradation of LSM cathode during long-term discharge. In order to improve the long-term stability of LSM cathode, it is of great importance to suppress the decrease of active TPB length due to current passage.

During long-term discharge at high operating temperature, LSM tends to react with YSZ to form insulating species at the contact region, such as $La_2Zr_2O_7$ and $SrZrO_3$, leading to the performance degradation of LSM cathode. Inserting an interlayer, usually doped ceria or zirconia, is often considered to avoid the interaction between LSM cathode and YSZ electrolyte [7,8]. However, the effect of the porous microstructure of interlayer on the long-term stability of cathode has not been elucidated clearly. It is expected that the employment of porous interlayer between the LSM cathode and YSZ electrode could maintain the active TPB length ratio after long-term discharge operation. In this work, therefore, a porous interlayer of YSZ or samarium-doped ceria was introduced between LSM cathode and YSZ electrolyte. The performance LSM cathodes before and after discharge were investigated by electrochemical impedance spectroscopy. The interface between LSM cathode and YSZ interlayer or electrolyte was three-dimensionally reconstructed by using FIB-SEM technology, and the effect of porous interlayer on the long-term stability of LSM cathode was discussed.

2. Experimental

Commercial 8 mol% Y_2O_3-stabilized ZrO_2 disk (YSZ, Tosoh Corp; thickness: 500 μm, diameter: 24 mm) was used as the electrolyte for the electrolyte-supported cells. The Ni/YSZ cermet anode with a composition of Ni:YSZ = 68:32 vol.% was prepared as described in our previous work [6]. 8 mol% Y_2O_3-stabilized ZrO_2 (YSZ, Tosoh Corp) and $Ce_{0.8}Sm_{0.2}O_{1.9}$ (SDC) powders were screen-printed on the YSZ electrolyte and subsequently fired at 1200 °C for 5 h to form the porous interlayer. The thickness of the interlayers was ca. 20 μm. The perovskite-type oxide of $(La_{0.8}Sr_{0.2})_{0.97}MnO_3$ (LSM) was screen-printed on the bare surface of YSZ electrolyte or on the interlayer and then calcined at 1150 °C for 5 h. The area of the working electrodes was ca. 0.283 cm^2. The thickness of the LSM cathode and Ni/YSZ anode was ca. 30 and 20 μm, respectively. Pure LSM cathode on bare YSZ electrolyte was denoted as LSM–YSZ_E. LSM cathode with porous YSZ interlayer (YSZ_I) and SDC interlayer (SDC_I) were denoted as LSM–YSZ_I and LSM–SDC_I, respectively. Platinum paste was painted to the side edge of the electrolyte and fired at 900 °C for 2 h as the reference electrode. The cells with these cathodes are illustrated in Fig. 1. The interface between LSM cathode and dense YSZ electrolyte, YSZ interlayer, and SDC interlayer is denoted as "the LSM–YSZ_E interface", "the LSM–YSZ_I interface", and "the LSM–SDC_I interface", respectively.

Prior to the electrochemical tests, the Ni/YSZ anode was reduced under H_2 atmosphere. Humidified hydrogen (95% H_2–5% H_2O) and pure oxygen were supplied to the anode and cathode with a flow rate of 100 mL min^{-1}, respectively. Discharge operation at 1.2 A cm^{-2} was carried out for the cells with LSM, LSM–YSZ_I, and LSM–SDC_I cathodes at 1000 °C. The terminal voltage of the cells throughout the discharge operation remained between 0.3 V and 0.5 V. The current density was extremely large and the temperature was out of the technically applicable range. As a result, the cathodes were actually tested under accelerated condition. The current was interrupted at the predetermined schedule to measure the electrochemical impedance spectrum between the cathode and reference electrode under the open circuit state using a Solartron 1260

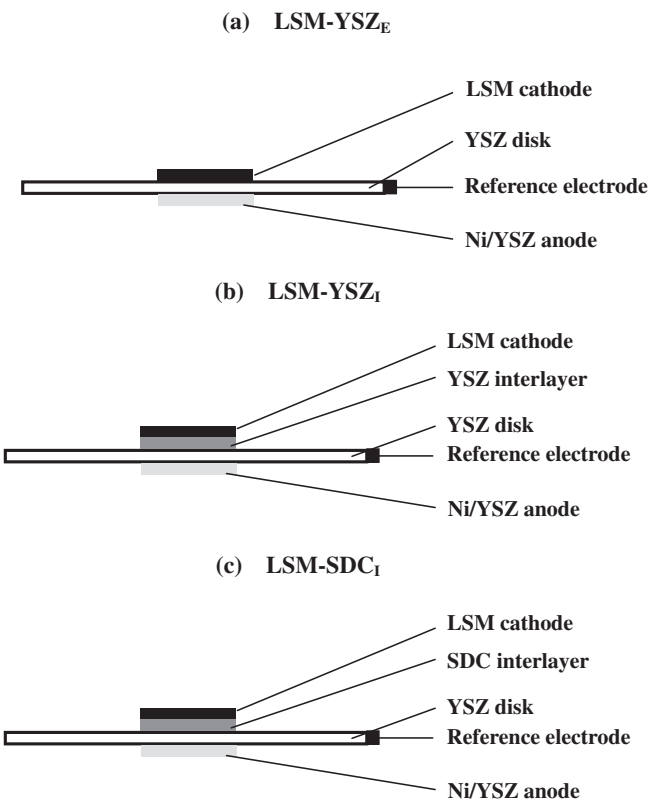

Fig. 1. Schematic illustration of three kinds of cathodes: (a) LSM–YSZ_E, (b) LSM–YSZ_I, and (c) LSM–SDC_I.

frequency response analyzer and a Solartron 1287 electrochemical interface. The frequency range was from 100 kHz to 0.1 Hz and the signal amplitude was 10 mV.

The microstructure of the cathodes before and after discharge operation was investigated by scanning electron microscope (SEM) equipped with energy-dispersive X-ray (EDX) spectrometer (Oxford). Three-dimensional (3D) observation of the interface between the cathode and interlayer was conducted by utilizing a dual-beam focused ion beam-scanning electron microscope (FIB-SEM, NVision 40, Carl Zeiss SMT-SIINT). The sample was embedded in epoxy resin (Marumoto Struers KK) under vacuum conditions until the pores in the sample were thoroughly filled. When the epoxy resin was solidified, the sample was cut and polished for observation. The set of cross-sectional SEM images (*xy*-plane) of the interface along the *z*-direction was obtained by sequential milling-and-observation operation. The phases of pore, LSM, and YSZ were three-dimensionally reconstructed and distinguished by the contrast. Detailed descriptions of the 3D reconstruction and quantitative analysis of the interfacial microstructure are given in Refs. [5,6,9]. The area-specific TPB length was defined as the TPB length per perspective area of *yz*-plane. TPB between closed pore, YSZ interlayer, and LSM cathode was regarded as inactive for oxygen reduction reaction. The composition of LSM near the LSM–SDC_I interface after discharge was investigated by energy-dispersive X-ray spectroscopy (EDX, JED-2300T, JEOL) in transmission electron microscope (TEM, JEM-2100F, JEOL).

3. Results and discussion

3.1. Effect of the YSZ interlayer on the long-term stability of the LSM cathode

The changes in the impedance spectra of LSM–YSZ_E and LSM–YSZ_I during discharge at 1.2 A cm^{-2} are shown in Fig. 2.

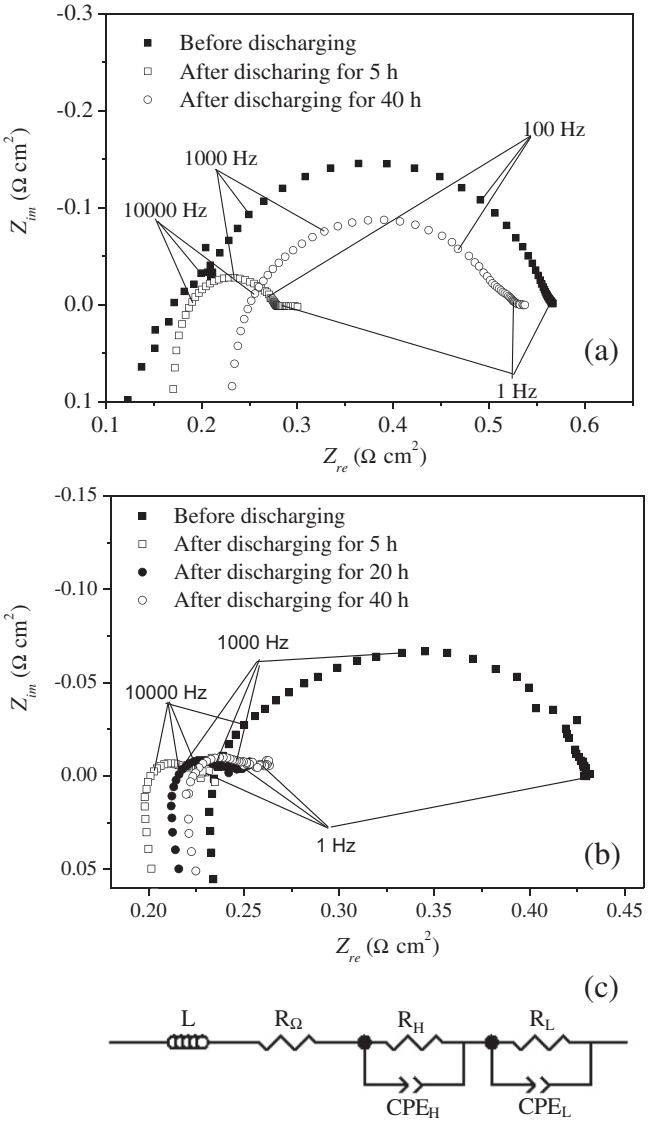

Fig. 2. Total, ohmic, and polarization resistances of LSM on (a) dense YSZ and (b) YSZ interlayer before and after discharge at 1.2 A cm^{-2}; temperature: 1000 °C.

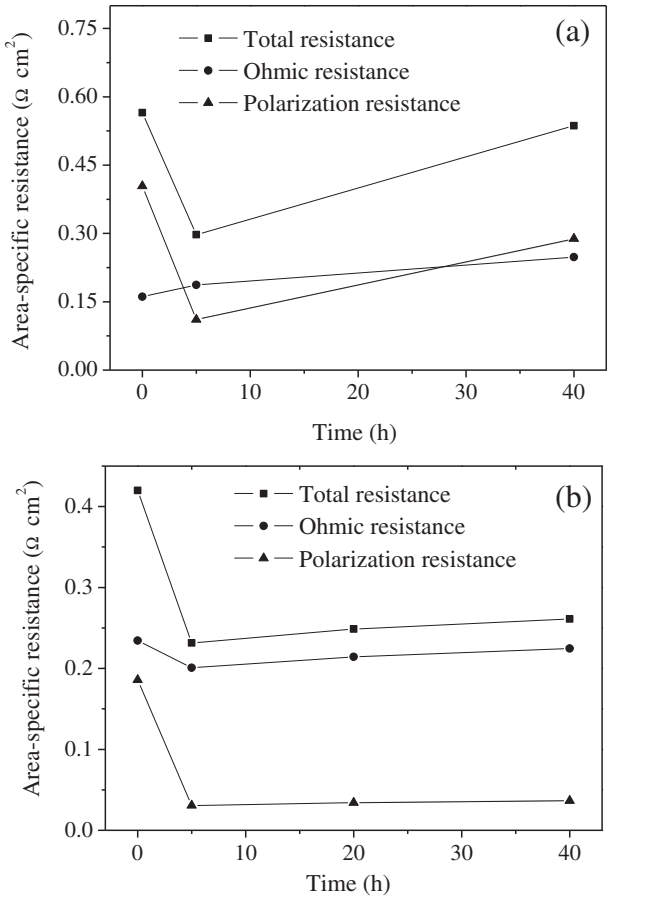

Fig. 3. The total, ohmic (R_Ω), and polarization resistance (R_p) during the discharge at 1.2 A cm^{-2} as a function of time.

Two semicircles are identified in the measured frequency range of 100,000–0.1 Hz. The impedance spectra were analyzed using the equivalent circuit in Fig. 2(c), where L is the inductance; R_Ω is the ohmic resistance between cathode and reference electrode; R_H, R_L, and CPE_H, CPE_L are the resistances and constant phase elements (CPEs) for the high- and low-frequency arcs. The total polarization resistance, R_p, is the sum of R_H and R_L.

The fitted R_Ω and R_P of LSM–YSZ_E and LSM–YSZ_I are plotted as a function of discharge time in Fig. 3. It is observed in Fig. 3(a) that the ohmic resistance of LSM–YSZ_E increased from 0.16 to 0.25 Ω cm^2 after discharge for 40 h, which should result from the formation of insulating phases, mainly zirconates, at the interface of LSM and YSZ [10]. On the other hand, the polarization resistance of LSM–YSZ_E changed much more severely than the ohmic resistance during discharge. It was reduced from 0.4 to 0.11 Ω cm^2 after discharge for 5 h, and then increased to 0.29 Ω cm^2 after discharge for 40 h. The reduction of polarization resistance of LSM–YSZ_E at the initial stage of cathodic polarization can be explained as follows. LSM is partially reduced under cathodic polarization. Simultaneously, oxygen vacancies are formed in the vicinity of triple phase boundary (TPB) of LSM cathode, YSZ electrolyte, and gas phase. As a result, LSM becomes partially ionic-conductive, and the active region for oxygen reduction reaction expands significantly [11–13]. When the current was interrupted, these oxygen vacancies decreased within a short time, which was sufficient for the electrochemical impedance measurement [11]. During the measurement, the impedance of LSM–YSZ_E increased with the gradual disappearance of oxygen vacancies. This explains the short line at the low-frequency region of the impedance spectrum of LSM–YSZ_E (indicated by an ellipse in Fig. 2(a)). Detailed discussion can be found in our previous work [11]. The subsequent deterioration of LSM cathode resulted from the microstructural change at the LSM–YSZ_E interface, which will be discussed afterwards.

In the case of LSM–YSZ_I (see Fig. 3(b)), the ohmic resistance reduced from 0.23 to 0.2 Ω cm^2 after discharge for 5 h, and then increased to 0.22 Ω cm^2 after 40 h. The polarization resistance of LSM–YSZ_I changed much more severely in the initial stage of discharge. The initial polarization resistance of LSM–YSZ_I was smaller than LSM–YSZ_E. It is considered that the combination of LSM and porous YSZ interlayer provides larger triple phase boundary of LSM, YSZ, and gas phase than that of LSM and dense YSZ electrolyte, resulting in the enhancement of initial performance. After discharge for 5 h, the polarization resistance of LSM–YSZ_I was reduced from 0.19 to 0.03 Ω cm^2. Subsequent discharge operation for 35 h only enlarged the polarization resistance of LSM–YSZ_I to 0.04 Ω cm^2. This increase in polarization resistance for LSM–YSZ_I was much smaller than that for LSM–YSZ_E. The results in Fig. 3 reveal that the polarization resistances dominated the polarization behaviors of LSM–YSZ_I and LSM–YSZ_E cathodes.

The microstructural changes of the LSM–YSZ_E and LSM–YSZ_I interface are shown in Fig. 4. As is shown in Fig. 4(a), the LSM–YSZ_E interface before discharge was composed of porous LSM layer and dense YSZ electrolyte. However, after discharge for 40 h, a dense layer was formed over YSZ (rectangle-selected area), accompanied with a large number of nanosized pores (designated by arrows) at the LSM–YSZ_E interface (Fig. 4(b)). Our group proposed that during discharge, LSM with A-site deficiency tended to migrate from the internal LSM–YSZ interface to the active TPB, leading to the formation of the thick and dense LSM layer over YSZ electrolyte [6].

The microstructure of LSM–YSZ_I interface before discharge is shown in Fig. 4(c). The particle size of YSZ in the interlayer was relatively smaller than LSM. After discharge for 40 h, some of LSM particles near the LSM–YSZ_I interface were connected by the dense layer (designated by a white ellipse in Fig. 4(d)), and nanosized pores appeared at the contact region of LSM cathode and YSZ interlayer (designated by an arrow in Fig. 4(d)). Therefore, it can be concluded that the microstructural change of LSM on YSZ interlayer during discharge was similar with that on dense YSZ electrolyte. The suppression of performance deterioration of LSM–YSZ_I should result from the porous microstructure of YSZ interlayer.

The 3-dimensionally reconstructed image of the LSM–YSZ_E interface region has been introduced in our previous work [6] and that of the LSM–YSZ_I interface is shown in Fig. 5. TPB lines of LSM, YSZ interlayer, and gas phase before and after discharge are illustrated on the surface of YSZ interlayer in Fig. 6. The active TPB is defined as the TPB among LSM, YSZ_I, and atmosphere while the inactive one is the TPB of LSM, YSZ_I, and closed pores. Before discharge, all of the TPB lines were active for oxygen reduction reaction. After discharge, despite of the appearance of some inactive TPB lines, the amount of active TPB lines increased significantly. A great number of short TPB branches, which resulted from the TPB of LSM, YSZ_I, and newly-formed pores, were observed.

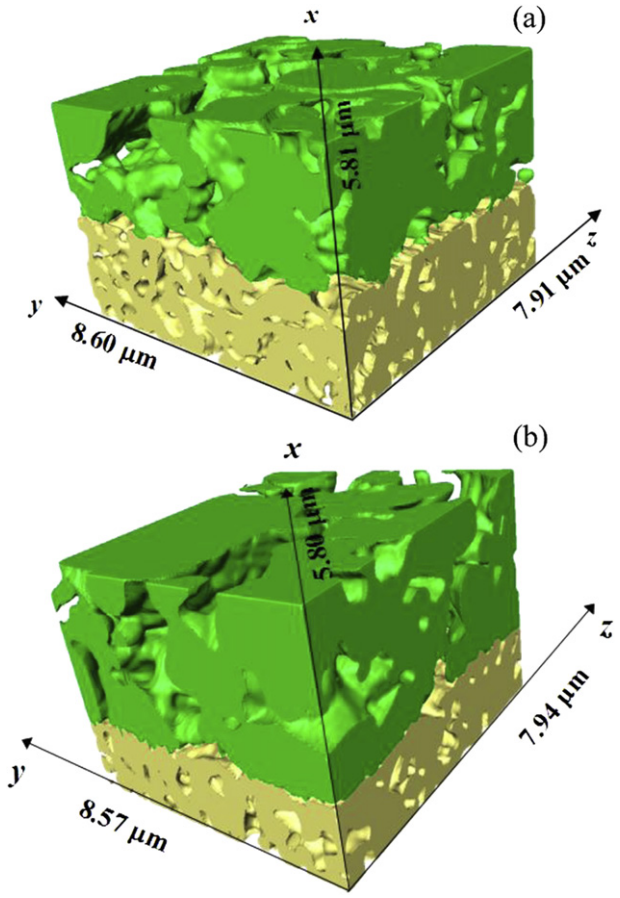

Fig. 5. Reconstructed LSM (green) on YSZ interlayer (yellow) (a) before and (b) after discharge at 1.2 A cm^{-2} for 40 h; temperature: 1000 °C.

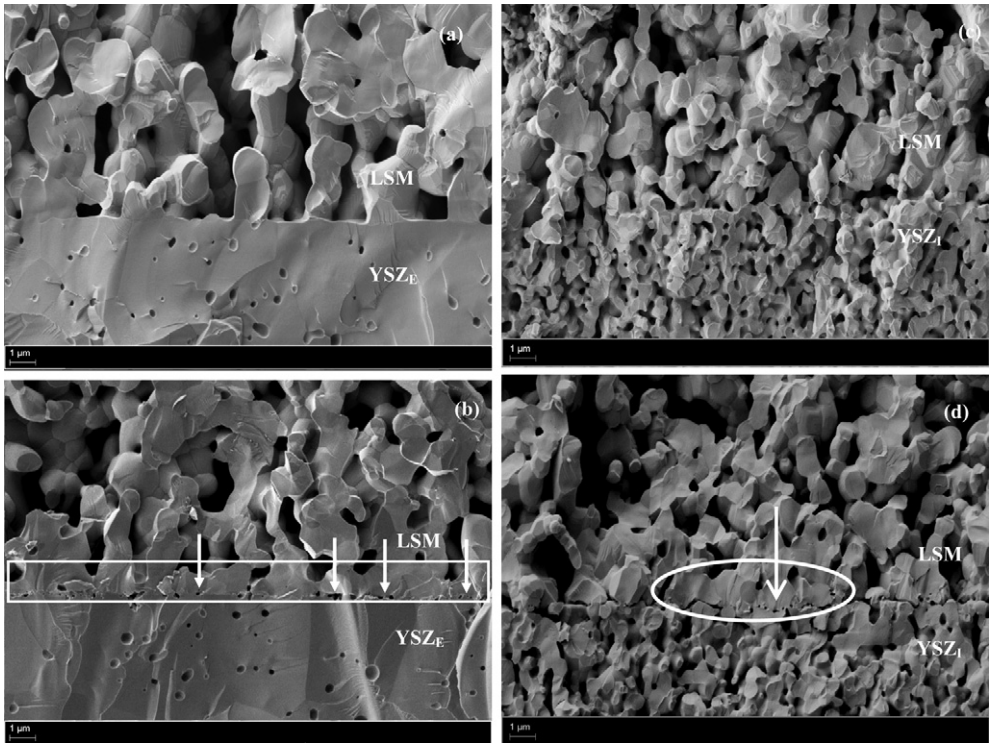

Fig. 4. SEM images of (a, c) LSM–YSZ_E and (b, d) LSM–YSZ_I: (a, b) before and (c, d) after discharge at 1.2 A cm^{-2} for 40 h; temperature: 1000 °C.

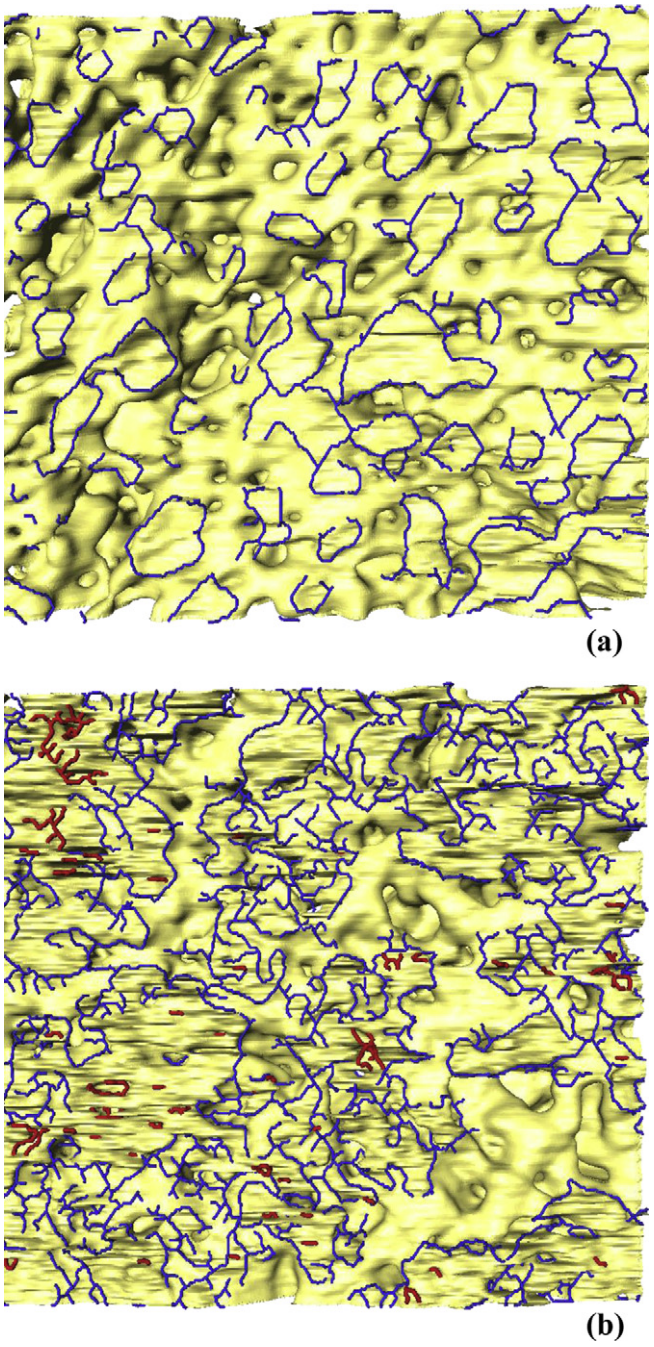

Fig. 6. Active (blue line) and inactive (red line) TPB on YSZ interlayer (a) before and (b) after discharge at 1.2 A cm^{-2} for 40 h; temperature: 1000 °C.

Table 1
Sample dimensions, spatial resolutions, and area-specific TPB length of LSM on YSZ interlayer before and after discharge at 1.2 A cm^{-2} for 40 h; temperature: 1000 °C.

Samples	Voxel size/nm			Sample dimension/μm			Area-specific TPB length[a]/μm $μm^{-2}$	
	x	*y*	*z*	*x*	*y*	*z*	Total	Active
Before discharge	27.9	27.9	43.8	5.81	8.60	7.91	2.45	2.45
After discharge	22.3	22.3	32.1	5.80	8.57	7.94	5.18	4.66

[a] Area-specific TPB length = real TPB length (μm)/(area of *yz*-plane, $μm^2$).

The quantitative analysis of the TPB length of LSM–YSZ_E and LSM–YSZ_I is shown in Table 1. For comparison, total and active area-specific TPB length of LSM–YSZ_E, which can be found in Ref. [6], and LSM–YSZ_I are plotted as a function of discharge time in Fig. 7. In Fig. 7(a), the total area-specific TPB length of LSM–YSZ_E before discharge was 1.22 μm $μm^{-2}$ and 100% active for oxygen reduction reaction. After discharge for 5 h, the total TPB length did not change while the active one decreased to 54%, which did not agree with the improved performance of LSM–YSZ_E after discharge for 5 h. This controversy has been explained in our previous work. The thickness of newly-formed LSM layer after discharge for 5 h was less than ca. 200 nm and thus could be ionic-conductive in the presence of oxygen vacancies. As a result, in addition to the active TPB length, more active reaction sites were generated on the surface of the newly-formed thin LSM layer. After discharge for 40 h, the active TPB length further decreased to 29%, and the newly-formed LSM layer was ca. 1.5 μm in thickness, which was too thick to be ion-conductive. Therefore, the performance of LSM–YSZ_E was degraded significantly comparing with that after discharge for 5 h [6].

In the case of LSM–YSZ_I cathode (see Fig. 7(b)), the initial total TPB length was 2.45 μm $μm^{-2}$ and active for the oxygen reduction reaction. This explained the superior performance of LSM–YSZ_I comparing with that of LSM–YSZ_E. After discharge at 1.2 A cm^{-2} at 1000 °C for 40 h, the total TPB length increased to 5.18 μm $μm^{-2}$. The newly-formed pores in the LSM–YSZ_I interface connected to the pores in the interlayer, and thus increased the active TPB length to 4.66 μm $μm^{-2}$ after discharge for 40 h, which still covered

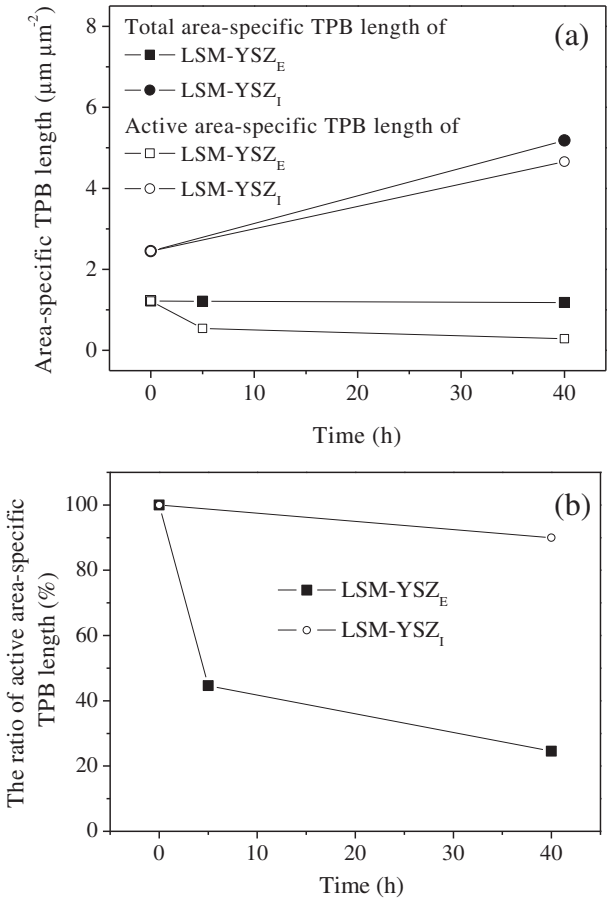

Fig. 7. Total and active area-specific TPB length of LSM–YSZ_E and LSM–YSZ_I as a function of time during discharge at 1.2 A cm^{-2}; temperature: 1000 °C.

approximately 90% of the total TPB length. As a result, the polarization resistance of LSM–YSZ_I did not increase after a long period of discharge operation. Therefore, it is proved that the use of porous YSZ interlayer was effective in preserving the active TPB length ratio for oxygen reduction reaction, and thus prevented the increase in the polarization resistance during discharge.

3.2. Effect of the SDC interlayer on the long-term stability of the LSM cathode

Doped ceria interlayer is often used to avoid the reaction between cathode and electrolyte. In this section, the effect of the porous SDC interlayer on the long-term stability of the LSM cathode was investigated.

Discharge operation at 1.2 A cm^{-2} was conducted on the cell with LSM–SDC_I cathode. The impedance spectra of LSM–SDC_I cathode during discharge are shown in Fig. 8. The impedance spectra were analyzed using the equivalent circuit in Fig. 8(b), where L' is the inductance; R'_Ω is the ohmic resistance between cathode and reference electrode; R'_H, R'_L, and CPE'_H, CPE'_L are the resistances and CPEs for the high- and low-frequency arcs. The total polarization resistance, R'_p, is the sum of R'_H and R'_L. The fitted total, ohmic, and polarization resistances are plotted as a function of time in Fig. 8(c). It is found that the ohmic resistance of LSM–SDC_I monotonically decreased with time while the polarization resistance decreased significantly during the initial 40 h and subsequently increased slightly after 160 h.

The microstructure of the LSM–SDC_I interface before discharge is shown in Fig. 9(a). The porous LSM and SDC layers can be clearly separated. After discharge at 1.2 A cm^{-2} at 1000 °C for 160 h, the LSM particles near the LSM–SDC_I interface agglomerated, as is indicated by a white ellipse in Fig. 9(b). The densification behavior of LSM on the SDC interlayer is quite similar with that observed for LSM–YSZ_I in Fig. 4(b).

The magnified image of LSM region near the LSM–SDC_I interface after discharge revealed that a large amount of nanoparticles with a diameter of 50–100 nm deposited on the grain boundary of LSM particles, as can be seen in Fig. 10(a). These nanoparticles can be discerned from the brighter contrast than the LSM particles in the backscattered electron image in Fig. 10(b). Another sample of LSM–SDC_I cathode was held under the open circuit state for 40 h and the microstructure of the LSM–SDC_I interface before and after the holding is shown in Fig. 11. After the operation, similar

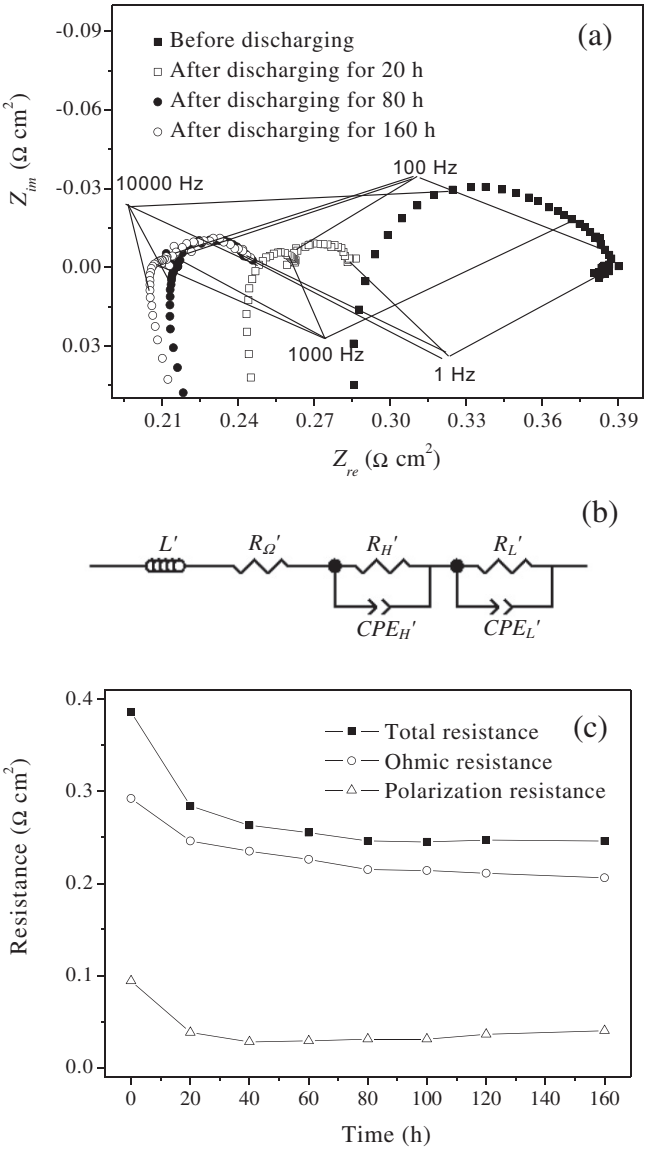

Fig. 8. (a) Impedance spectra of LSM on the SDC interlayer before and after discharge at 1.2 A cm^{-2} for 160 h; (b) The total, ohmic, and polarization resistances as a function of time calculated from (a); temperature: 1000 °C.

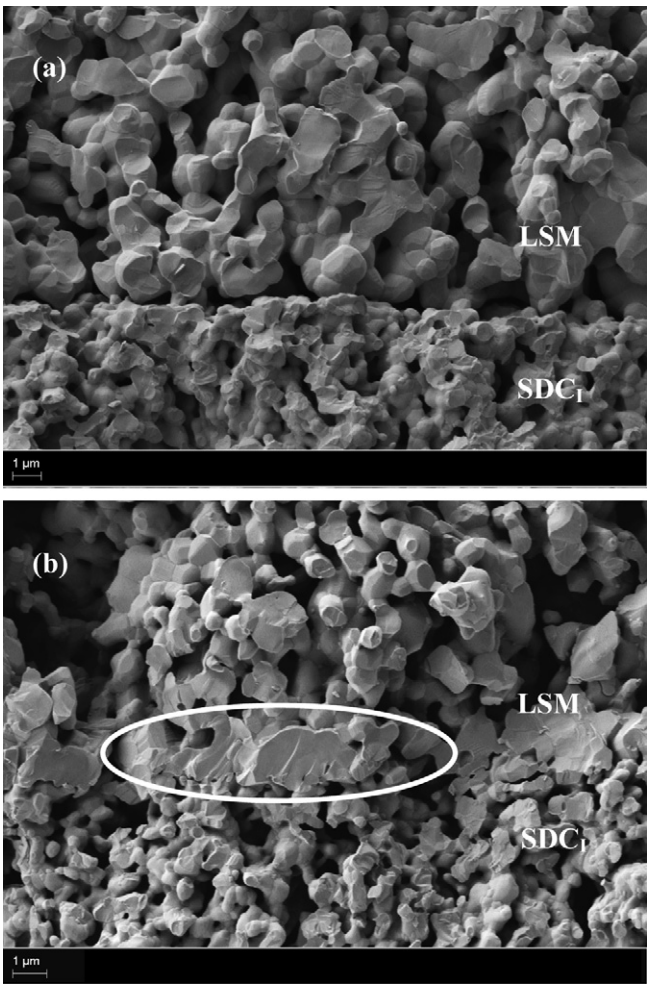

Fig. 9. SEM images of the LSM–SDC_I interface (a) before and (b) after discharge at 1.2 A cm^{-2} for 160 h; temperature: 1000 °C.

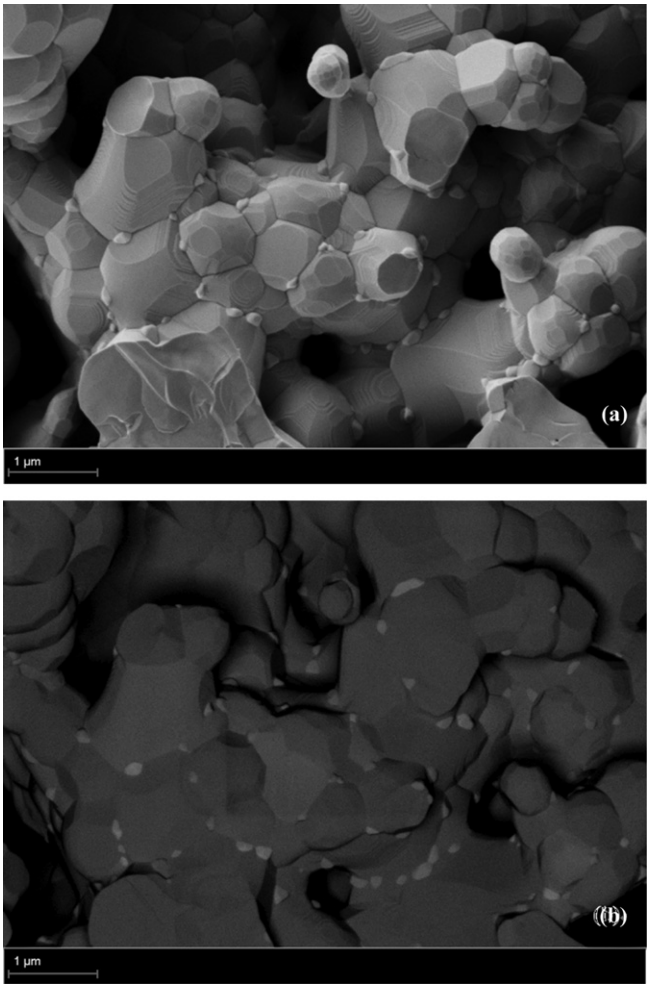

Fig. 10. (a) Secondary electron and (b) backscattered electron images of LSM near the LSM–SDC_I interface after discharge at 1.2 A cm^{-2} for 160 h; temperature: 1000 °C.

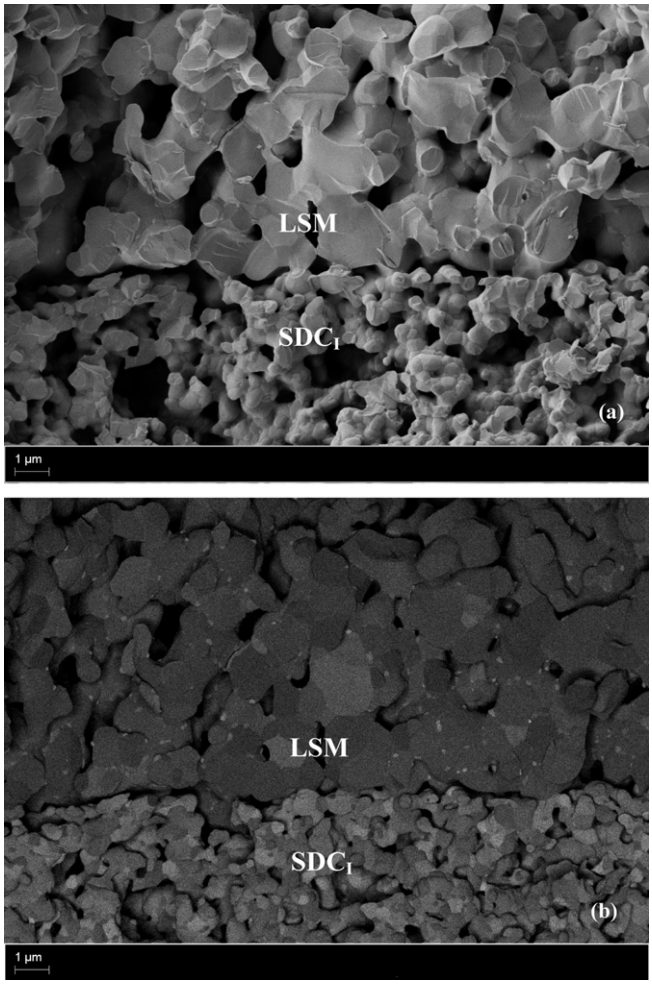

Fig. 11. (a) Secondary electron and (b) backscattered electron images of LSM on SDC interlayer after holding at open circuit state for 40 h; temperature: 1000 °C.

nanoparticles were observed around the LSM–SDC_I interface. Therefore, the nanoparticles were formed along the grain boundary of LSM regardless of the current passage.

The compositional analysis for the nanoparticles mentioned above was conducted by TEM–EDX. The TEM image of LSM–SDC_I sample after discharge at 1.2 A cm^{-2} for 40 h is shown in Fig. 12. Relatively large particles are ascribed to LSM and small particles to SDC. The white circled area is the LSM–SDC_I interface. Local compositional analysis was conducted with EDX on the squared area. Because the characteristic peaks of Sm in the EDX spectra were overlapped by those of other metallic elements, the quantitative analysis of Sm was not reliable. Therefore, the distribution and migration of Sm are not discussed in this work. The positions for the EDX analysis are marked in Fig. 13. The nanoparticles were located at the grain boundary of LSM. The analysis points 1 and 2 are on the nanoparticles and positions 3 and 4 on the bulk of LSM. As summarized in Table 2, the nanoparticles located on positions 1 and 2 contained a large amount of Ce and no Ce was detected from the LSM region (positions 3 and 4). One possible mechanism for the formation of Ce-rich nanoparticles on the grain boundary of LSM can be interpreted as follows. CeO_2 has some solubility in LSM lattice, which increased with temperature [14]. The interlayer of SDC was fired on the YSZ disk at 1200 °C. At the testing temperature (1000 °C), the solubility of CeO_2 was lower than that at 1200 °C. As a result, CeO_2 segregated at the grain boundary of LSM gradually

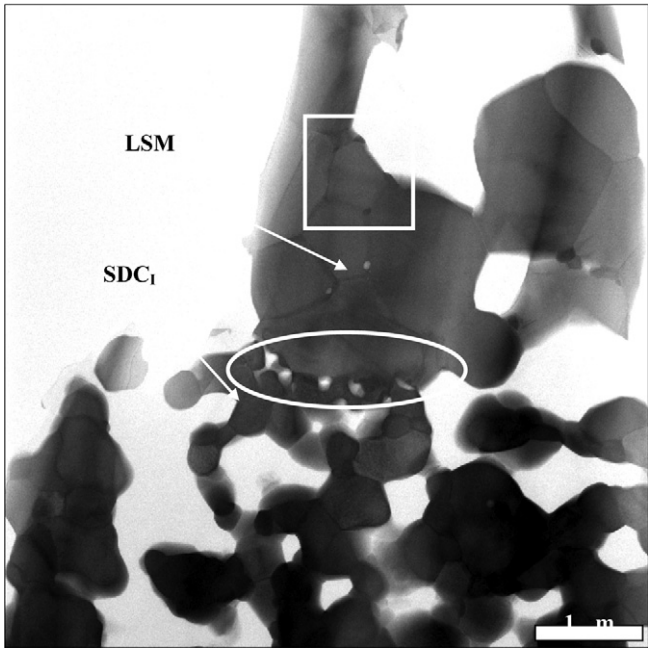

Fig. 12. TEM image of the LSM–SDC_I interface after discharge at 1.2 A cm^{-2} for 40 h; temperature: 1000 °C.

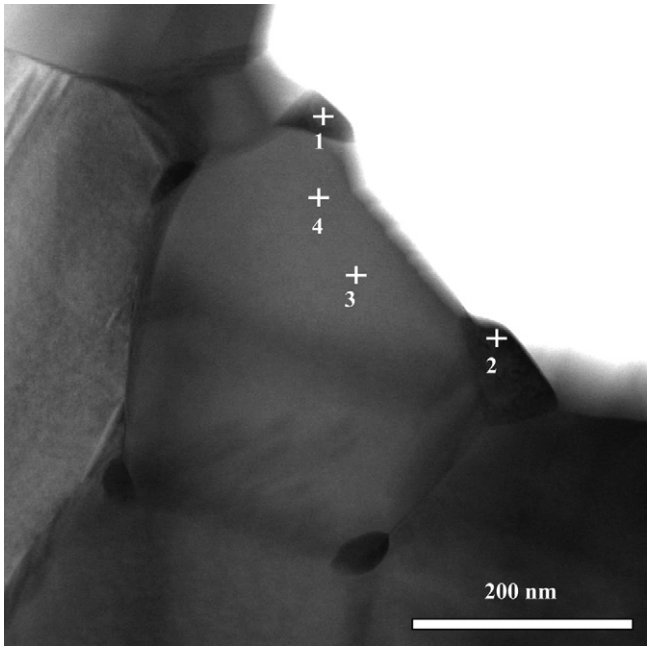

Fig. 13. TEM image of the rectangle-selected area in Fig. 12.

Table 2
EDX point analysis at positions 1–4 in Fig. 13.

Elements	1 (%)	2 (%)	3 (%)	4 (%)
Mn	18.3	17.6	51.2	51.3
Sr	5.5	4.3	10.9	10.7
La	18.1	12.0	37.9	38.0
Ce	55.9	63.1	–	–
Sm	2.2	3.0	–	–
Total	100	100	100	100

and formed the small particles mentioned above. It was reported that even a small amount of CeO_2 added into $La_{0.8}Sr_{0.2}MnO_3$ cathode significantly reduced the ohmic and polarization resistances [14,15]. Therefore, the formation of Ce-contained particles on the grain boundary of LSM should contribute to the enhancement of the long-term performance of LSM–SDC_I cathode.

4. Conclusions

In summary, it was confirmed that employing a porous YSZ interlayer would significantly improve the long-term stability of LSM cathodes even under current-accelerated condition. Because of the porous morphology of interlayer, the active TPB length ratio for LSM–YSZ_I cathode maintained 90% even after discharge at 1.2 A cm^{-2} for 40 h, and thus the increase in the polarization resistance was prevented. On the other hand, the LSM cathode with a porous SDC interlayer showed even better long-term stability. Interestingly, both of the ohmic and polarization resistance was decreased after discharge at 1.2 A cm^{-2} for 160 h. The decrease in the ohmic resistance of LSM–SDC_I should be related with the formation of Ce-rich particles on the LSM grain boundary. Further investigation is needed to elucidate the effect of Ce on improving the long-term stability of LSM cathode.

Acknowledgment

This work was supported by New Energy and Industrial Technology Development Organization (NEDO), Japan (Development of System and Elemental Technology on Solid Oxide Fuel Cell).

References

[1] X.B. Chen, B. Hua, J. Pu, J. Li, L. Zhang, S.P. Jiang, Int. J. Hydrogen Energy 34 (2009) 5737–5748.
[2] S. Miyoshi, J.O. Hong, K. Yashiro, A. Kaimai, Y. Nigara, K. Kawamura, T. Kawada, J. Mizusaki, Solid State Ionics 154–155 (2002) 257–263.
[3] F.L. Liang, J. Chen, S.P. Jiang, B. Chi, J. Pu, J. Li, Electrochem. Commun. 11 (2009) 1048–1051.
[4] I. Yasuda, K. Ogasawara, M. Hishinuma, T. Kawada, M. Dokiya, Solid State Ionics 86–88 (1996) 1197–1201.
[5] T. Matsui, Y. Mikami, H. Muroyama, E. Koichi, J. Electrochem. Soc. 157 (2010) B1790–B1794.
[6] J. Yang, H. Muroyama, T. Matsui, K. Eguchi, J. Power Sources 204 (2012) 25–33.
[7] M. Juhl, S. Primdahl, C. Manon, M. Mogensen, J. Power Sources 61 (1996) 173–181.
[8] E. Ivers-Tiffee, A. Weber, D. Herbstritt, J. Eur. Ceram. Soc. 21 (2001) 1805–1811.
[9] H. Iwai, N. Shikazono, T. Matsui, H. Teshima, M. Kishimoto, R. Kishida, D. Hayashi, K. Matsuzaki, D. Kanno, M. Saito, H. Muroyama, K. Eguchi, N. Kasagi, H. Yoshida, J. Power Sources 195 (2010) 955–961.
[10] M.C. Brant, T. Matencio, L. Dessemond, R.Z. Domingues, Chem. Mater. 13 (2001) 3954–3961.
[11] J. Yang, H. Muroyama, T. Matsui, K. Eguchi, Int. J. Hydrogen Energy 35 (2010) 10505–10512.
[12] H.Y. Lee, W.S. Cho, S.M. Oh, J. Electrochem. Soc. 142 (1998) 2659–2664.
[13] Y. Jiang, S. Wang, Y. Zhang, J. Yan, W. Li, J. Electrochem. Soc. 145 (1998) 373–378.
[14] E. Konysheva, S.M. Francis, J.T.S. Irvine, J. Electrochem. Soc. 157 (2010) B159–B165.
[15] J.P. Wiff, K. Jono, M. Suzuki, S. Suda, J. Power Sources 196 (2011) 6196–6200.